

## Electronic Supplementary Information

**Enzyme cascade-amplified immunoassay based on the nanobody-alkaline phosphatase fusion and MnO<sub>2</sub> nanosheets for the detection of ochratoxin A in coffee**

Zeling Zhang,<sup>a</sup> Benchao Su,<sup>a</sup> Huan Xu,<sup>a</sup> Zhenyun He,<sup>b</sup> Yuling Zhou,<sup>c</sup> Qi Chen,<sup>a</sup> Zhichang Sun,<sup>a</sup> Hongmei Cao <sup>a</sup> and Xing Liu <sup>\*a</sup>

<sup>a</sup> *School of Food Science and Engineering, Hainan University, 58 Renmin Avenue, Haikou 570228, China. E-mail: zhangzeling@hainanu.edu.cn, benchao312@hainanu.edu.cn, xuhuan.hnu@foxmail.com, qichen@hainanu.edu.cn, sunzhichang11@163.com, hmcao@hainanu.edu.cn*

<sup>b</sup> *Hainan College of Economics and Business, Haikou 571129, China. E-mail: zhenyun89@foxmail.com*

<sup>c</sup> *Hainan Institute for Food Control, Haikou 570314, China. E-mail: zhouyuling0607@163.com*

## Contents

Table S1.....	S-3
Figure S1.....	S-4
Synthesis and characterization of MnO <sub>2</sub> nanosheets.....	S-5
Figure S2.....	S-6
Figure S3.....	S-7
Figure S4.....	S-8
Optimization of the colorimetric sensing system for mNb-AP.....	S-9
Figure S5.....	S-10
Table S2.....	S-11
Figure S6.....	S-12
Table S3.....	S-13
Matrix effect.....	S-14
Table S4.....	S-15
Table S5.....	S-16
References.....	S-17

**Table S1.** Primers for the construction of recombinant expression vector for mNb-AP

Primers	Sequence (5'-3')
NA-NF	CCCAAGCTTCAGTTGCAGCTCGTGGAGTC
NA-NR	AGAGCCACCTCCGCCTGAACCGCCTCCTCCTTGTGGTTTTGGTGTCTT
NA-AF	G TTCAGGCGGAGGTGGCTCTGGCGGTGGCGGATCCACACCAGAAATG CCTGTTCTG
NA-AR	CCGCTCGAGTTTCAGCCCCAGAGCGGCTTTCATG

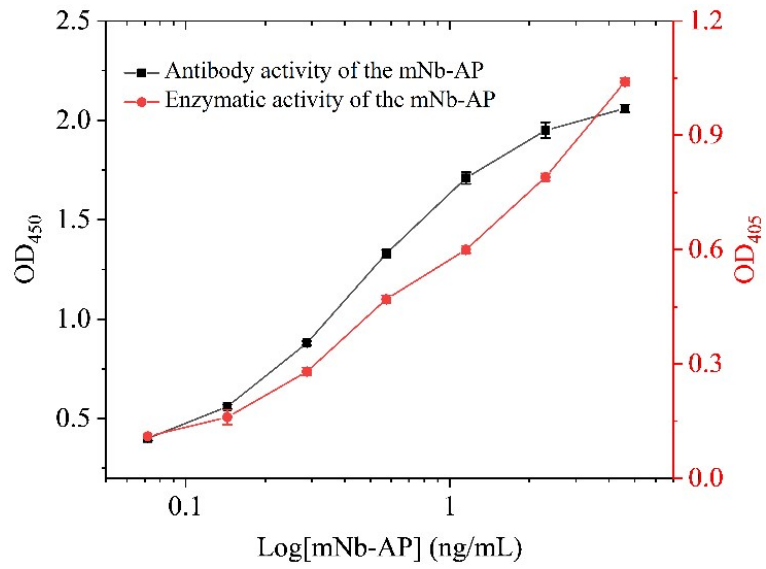


**Figure S1.** Analysis of antibody activity and enzymatic activity of the mNb-AP by an indirect ELISA. Error bars denote the standard deviations of three independent experiments.

### **Synthesis and characterization of MnO<sub>2</sub> nanosheets**

The MnO<sub>2</sub> nanosheets were synthesized by the redox method as reported previously with some modifications<sup>1</sup>. Briefly, 20 mL TMA-OH (0.6 M) solution and 2 mL 30% (m/v) H<sub>2</sub>O<sub>2</sub> was promptly mixed with 10 mL MnCl<sub>2</sub> solution (0.3 M). The resultant dark brown solution was constantly stirred overnight at room temperature. The precipitates of MnO<sub>2</sub> nanosheets were collected by centrifugation and dried in a 60°C oven after washing with methanol and ultra-pure water. The dried MnO<sub>2</sub> nanosheets were dispersed in deionized water, and the supernatant was obtained by centrifugation (1500g, 20 min) after ultrasonic exfoliation for 12 h. The prepared MnO<sub>2</sub> nanosheets solution was quantified according to Lambert-Beer's law. Tests including TEM, AFM, and zeta-potential analysis were performed to characterize the morphology and stability of MnO<sub>2</sub> nanosheets. The TEM image of the MnO<sub>2</sub> nanosheets exhibits a typical two-dimensional layer structure with multiple folds and crinkles with an average diameter of approximately 700 nm (Figure S2A), and the thickness of the nanosheets was determined to be around 2.5 nm by the AFM test (Figure S2B). Furthermore, a negative zeta potential of -34.07 mv was measured by the Zetasizer nano analyzer for the nanosheets dispersion, demonstrating that the nanosheets have a negatively charged surface which could contribute to acquiring good water dispersibility (Fig. S2C). Thus, the results indicated that the MnO<sub>2</sub> nanosheets were prepared with good morphology and stability.

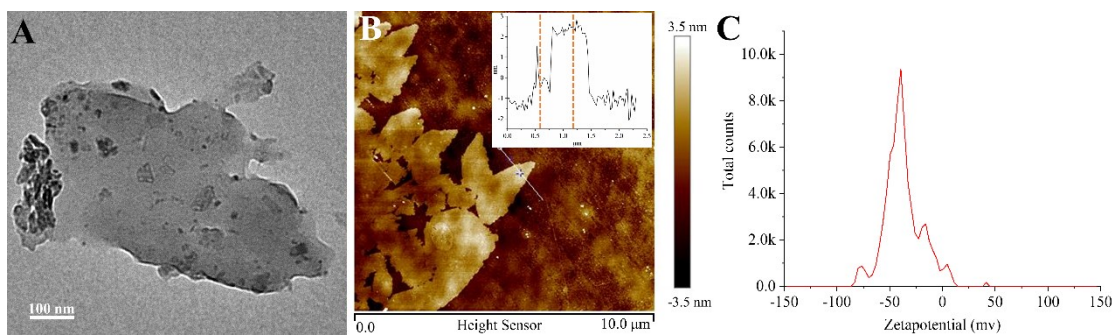


**Figure S2.** Morphology and stability analysis of the MnO<sub>2</sub> nanosheets. (A) TEM, (B) AFM, and (C) zeta potential.

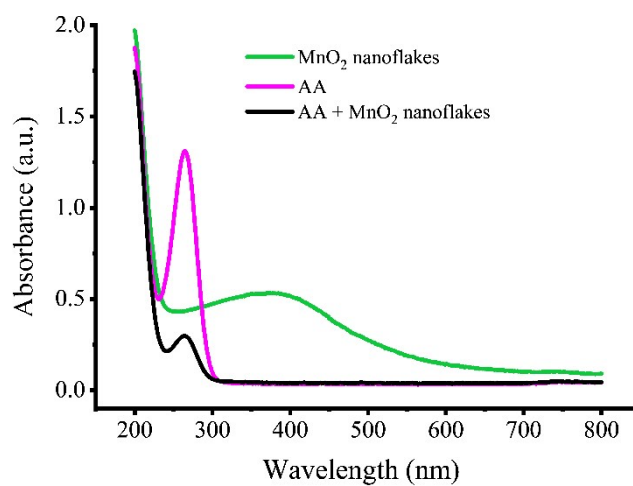


**Figure S3.** UV-vis absorption spectra of MnO<sub>2</sub> nanosheets, AA, and MnO<sub>2</sub> nanosheets + AA. The experimental conditions are listed below: 55  $\mu$ M MnO<sub>2</sub> nanosheets, 150  $\mu$ M AA, 50 mM Tris-HCl with 5 mM MgCl<sub>2</sub> (pH 10.0), and 40 mM NaAc-HAc (pH 3.8).

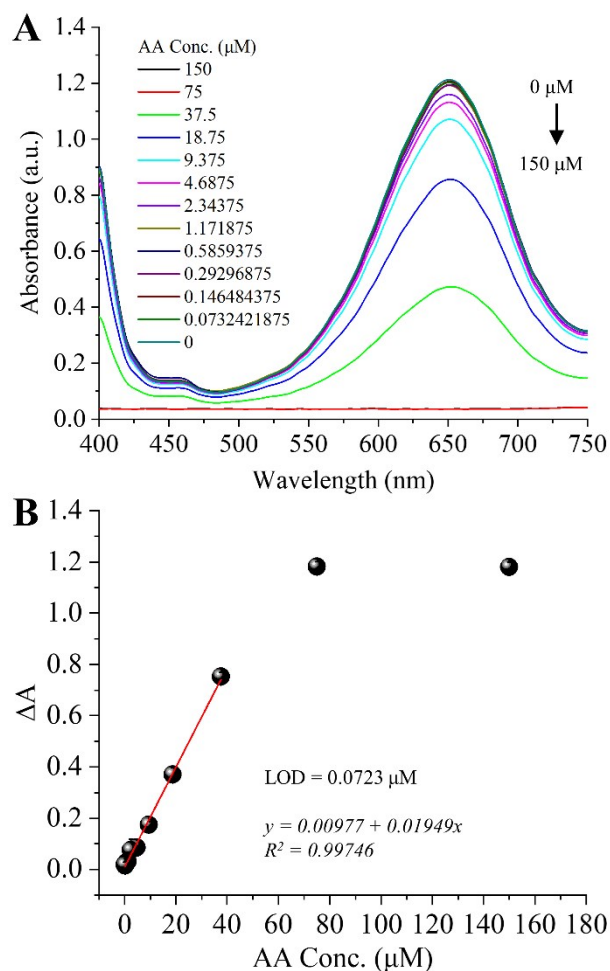


**Figure S4.** Absorption spectra of the  $\text{MnO}_2$  nanosheets/TMB solution of the colorimetric sensing system induced by various concentrations of AA (**A**) and the relationship between the difference of absorbance at 650 nm and the AA concentration (**B**). Inset: calibration plot of the difference of absorbance at 650 nm ( $\Delta A$ ) versus concentration of AA ( $\Delta A = A_0 - A$ , where  $A_0$  and  $A$  represent the absorbance of the colorimetric sensing system at 650 nm in the absence and presence of AA, respectively). Error bars denote the standard deviations of three independent experiments. The experimental conditions are listed below: 160  $\mu\text{M}$  TMB, 11.25  $\mu\text{M}$   $\text{MnO}_2$  nanosheets, 200 mM NaAc-HAc buffer (pH 4.5).

### **Optimization of the colorimetric sensing system for mNb-AP**

To obtain the best detection performance of the colorimetric sensing system, various experimental conditions including the MnO<sub>2</sub> nanosheets Conc., AAP Conc., incubation time of MnO<sub>2</sub> nanosheets, and incubation time of AAP were systematically optimized. The difference of absorbance at 650 nm ( $\Delta A = A_0 - A$ ) was used as the criteria, where  $A_0$  and  $A$  represent the absorption intensity of the colorimetric system at 650 nm in the absence and presence of AP. Figure S5A shows that the  $\Delta A$  value gradually rose with the increased concentration of MnO<sub>2</sub> nanosheets in the range of 0.35-1.1 mM and declined with the further increased nanosheets concentration. Because of the top value of  $\Delta A$ , 1.1 mM of MnO<sub>2</sub> nanosheets was selected for further research. Similarly, the optimum concentration of AAP was determined as 150 mM (Figure S5B). As seen in Figure S5C, the  $\Delta A$  value slightly decreased with the increase of incubation time of MnO<sub>2</sub> nanosheets, and 150 s of incubation time was selected for the highest  $\Delta A$  value. Figure S5D shows that the incubation time of APP can significantly influence the assay performance and the optimal incubation time was determined to be 90 min owing to the largest  $\Delta A$  value. Thus, the optimum working conditions for the colorimetric sensing system were shown below: MnO<sub>2</sub> nanosheets Conc., 1.1 mM; AAP Conc., 150 mM; incubation time of MnO<sub>2</sub> nanosheets, 150 s; incubation time of AAP, 90 min.

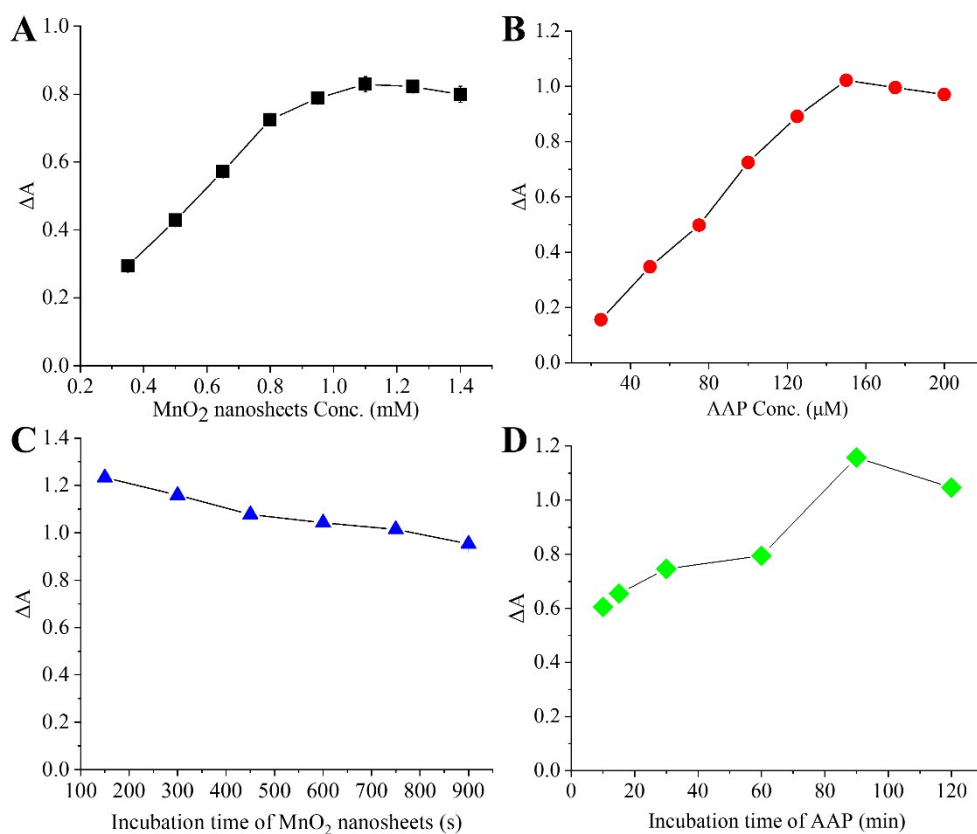


**Figure S5.** Optimization of the colorimetric sensing system of mNb-AP. **(A)**  $\text{MnO}_2$  nanosheets Conc.: 0.35, 0.5, 0.65, 0.8, 0.95, 1.1, 1.25, 1.4 mM; **(B)** AAP Conc.: 25, 50, 75, 100, 125, 150, 175, 200  $\mu\text{M}$ ; **(C)** Incubation time of  $\text{MnO}_2$  nanosheets: 150, 300, 450, 600, 750, 900 s; **(D)** Incubation time of AAP: 10, 15, 30, 60, 90, 120 min. The error bars denote the standard deviations of three independent experiments.

**Table S2.** Optimization of the concentrations of OTA-BSA and mNb-AP by the checkerboard titration

mNb-AP ( $\mu\text{g}/\text{mL}$ )	OTA-BSA ( $\mu\text{g}/\text{mL}$ )		
	2	1	0.5
4	11.5	12.2	12.0
2	11.9	12.4	13.7
1	18.1	14.9	16.92
0.5	15.3	11.9	14.1
0.25	3.84	3.35	3.80
0.125	1.91	1.85	2.00
0.0625	1.36	1.40	1.39

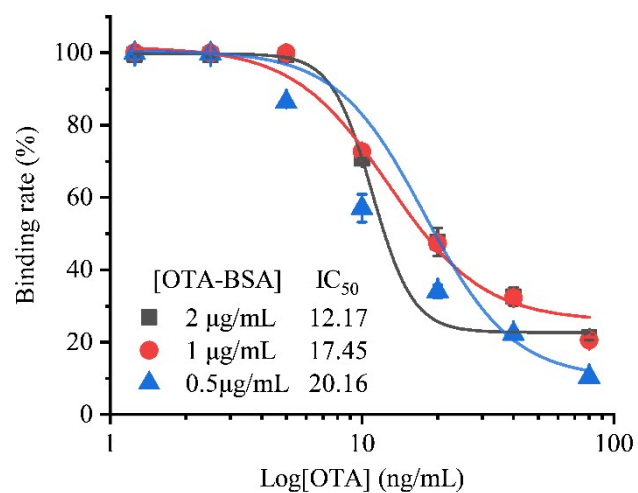


**Figure S6.** Optimization of the coating antigen concentration by the indirect competitive ELISA. The error bars denote the standard deviations of three independent experiments.

**Table S3.** Analytical performance comparison of the ECAIA with other reported methods based on nanomaterials for detecting OTA

Materials	LOD (ng/mL)	Linear range (ng/mL)	Time (min)	Ref.
Au@Fe <sub>3</sub> O <sub>4</sub>	0.03	0.5-100ng/mL	75	2
AuNPs	8.08	8.08-252.5	5	3
AuNPs	20	32-1024	25	4
Hemin/G-quadruplex	$2.6 \times 10^{-4}$	0.001-0.5	180	5
MnO <sub>2</sub> nanosheets, Nb-AP	3.38	4.55-12.85	132.5	This work

### **Matrix effect**

To reduce the matrix effect from the coffee samples, various proteins including 1% bovine serum albumin (BSA), 1% ovalbumin (OVA), 1% skim milk powder (SMP) and 1% gelatin were used to dilute the coffee extracts for shielding the matrix interference. The diluted extracts were used to prepare the OTA standards (3.33 ng/mL) for analysis by the developed ECAIA and the obtained binding rates were compared with that of the standard (3.33 ng/mL) in the standard assay buffer without matrix. As shown in Table S3, the OTA standards spiked in the coffee extract that was diluted with 1% SMP exhibited the lowest difference of binding rate, indicating the strongest shielding effect of 1% SMP among the four tested shielding proteins. On this basis, the shielding effects of different concentrations of SMP were also investigated. As seen in Table S4, the lowest difference of binding rate (-0.015) was observed from the group of OTA standard spiked in the coffee extract that was diluted 20 times with 2% SMP. This indicated that the matrix effect from the coffee extract could be minimized by 20-fold dilution using 2% SMP.

**Table S4.** Evaluation of the effects of different shielding reagents on reducing matrix interference from coffee

Shielding reagent	Difference of binding rate <sup>a</sup>		
	1/10 extract	1/20 extract	1/30 extract
1% BSA	0.207	0.343	0.263
1% OVA	0.169	0.154	0.379
1% fish gelatin	0.152	0.246	0.399
1% SMP	0.129	0.120	0.088

<sup>a</sup>The difference of binding rates between OTA standard (3.33 ng/mL) in assay buffer without matrix and that in coffee extract dilutions prepared with various shielding reagents

**Table S5.** Optimization of the concentration of SMP

SMP Conc. (%)	Difference of binding rate <sup>a</sup>		
	1/10 extract	1/20 extract	1/30 extract
4	0.021	-0.357	-0.172
2	-0.135	-0.015	-0.141
1	-0.080	0.033	-0.313
0.5	-0.226	-0.253	-0.237

<sup>a</sup>The difference of binding rates between OTA standard (3.33 ng/mL) in assay buffer without matrix and that in coffee extract dilutions prepared with different concentrations of SMP

## References

1. J. Liu, L. Meng, Z. Fei, P. J. Dyson, X. Jing and X. Liu, *Biosensors and Bioelectronics*, 2017, **90**, 69-74.
2. C. Wang, J. Qian, K. Wang, X. Yang, Q. Liu, N. Hao, C. Wang, X. Dong and X. Huang, *Biosensors and Bioelectronics*, 2016, **77**, 1183-1191.
3. C. Yang, Y. Wang, J.-L. Marty and X. Yang, *Biosensors and Bioelectronics*, 2011, **26**, 2724-2727.
4. X. Yin, S. Wang, X. Liu, C. He, Y. Tang, Q. Li, J. Liu, H. Su, T. Tan and Y. Dong, *Analytical sciences : the international journal of the Japan Society for Analytical Chemistry*, 2017, **33**, 659-664.
5. M. Wei and W. Zhang, *Sensors and Actuators B: Chemical*, 2018, **276**, 1-7.